Exploring Three-Dimensional Spatiotemporal Distribution of Aerosols in the Sichuan Basin

Hu, C.,[1,2] Lim, H. S.,[1*] Zhang, H.,[2] Zhang Y.[1,2] and Zhang, R.,
[1]School of Physics, Universiti Sains Malaysia, 11800, Penang, Malaysia
E-mail: huchengyu@student.usm.my, hslim@usm.my,* zhangyuanjun@student.usm.my, zhangrui8585@student.usm.my
[2]Sichuan Water Conservancy Vocational College, 611231, Chengdu, China, E-mail: zhhr01@gmail.com
**Corresponding Author*

DOI: https://doi.org/10.52939/ijg.v21i5.4155

Abstract
This study investigates the three-dimensional spatiotemporal distribution of aerosols in the Sichuan Basin from 2006 to 2023 using data from the CALIPSO satellite. Taking advantage of CALIPSO's high-resolution vertical and nighttime detection capabilities, the research provides a comprehensive analysis of aerosol optical depth (AOD), vertical structure, and aerosol type composition within the basin. The results reveal a distinct "high internal, low peripheral" AOD distribution pattern shaped by the basin's topography. Overall AOD levels exhibited a declining trend, decreasing from approximately 0.4 in 2006 to around 0.3 in 2023. Seasonal variations show AOD peaks in summer and autumn, while winter is characterized by localized pollutant accumulation. Vertically, aerosols are primarily concentrated within the 0–3 km layer, with larger particles found below 5 km during the day and between 3–8 km at night. The proportions of aerosol species remained relatively stable across seasons and altitudes, indicating limited variability in aerosol types. Biomass fuel combustion and human activities are identified as the main sources of aerosols in the region. This study offers valuable insights into aerosol distribution dynamics in enclosed terrain regions and provides a scientific foundation for future research. Further work is recommended to quantitatively examine the driving forces behind aerosol distribution patterns, including meteorological, industrial, and climatic factors.

Keywords: Aerosol Optical Depth (AOD), Sichuan Basin, CALIPSO, Vertical Distribution, Spatiotemporal Analysis

1. Introduction

Basins, as enclosed terrain systems, foster unique meteorological and atmospheric conditions due to their topographic constraints, which often lead to weak horizontal airflow, temperature inversions, and pollutant accumulation. These characteristics make basins particularly susceptible to persistent aerosol pollution and adverse air quality events. Understanding aerosol distribution within basin environments is thus crucial for accurate climate modelling, effective air pollution control, and regional environmental management [1]. Over the past two decades, numerous studies have utilized passive remote sensing techniques particularly the Moderate Resolution Imaging Spectroradiometer (MODIS) to examine the horizontal distribution and seasonal variations of aerosols in various basins. For instance, one study analysed seasonal aerosol dynamics in the Mediterranean Basin using MODIS data, highlighting the role of different aerosol types [2]. Another study validated MODIS-derived aerosol optical depth (AOD) against AERONET observations in the Ganges Basin [3]. Subsequent work expanded on this by assessing six-year AOD trends across the Mediterranean region [4]. More recently, long-term AOD trends in the Sichuan Basin have been examined using MODIS data, emphasizing the severe pollution levels in this enclosed basin [5]. However, while these studies have significantly advanced the understanding of aerosol behaviour in horizontal dimensions, they largely overlooked the vertical structure of aerosols an essential component for interpreting transport processes, radiation interactions, and pollution mechanisms. Moreover, passive sensors like MODIS are limited to daytime observations, leaving a critical gap in understanding aerosol dynamics during nighttime hours.

To address these limitations, the Cloud Aerosol Lidar and Infrared Pathfinder Satellite Observations (CALIPSO) mission, launched in 2006, offers a powerful alternative by providing active remote sensing of aerosol vertical profiles on a global scale, both during the day and at night [6][7] and [8]. CALIPSO enables detailed three-dimensional characterization of aerosol layers, including their altitude, thickness, and type. Building on this capability, recent studies have explored the vertical distribution of aerosols across China. For example, a number of studies have utilized CALIPSO data to explore vertical aerosol distributions at the regional scale [9][10] and [11]. Others have focused on understanding aerosol layering and variations in elevation, especially in southwestern China and in areas with complex mountainous terrain [12] and [13]. However, these investigations mainly targeted broader geographical regions and did not explicitly address the distinct dynamics within basin environments, where vertical transport and pollutant trapping behave differently due to closed topography.

To fill this research gap, the present study focuses on the Sichuan Basin a typical basin in southwestern China known for its persistent haze and complex atmospheric conditions. Utilizing CALIPSO satellite lidar data, we conduct a comprehensive analysis of the three-dimensional spatiotemporal distribution of aerosols in the basin. Our study goes beyond previous work by integrating vertical, seasonal, and diurnal dimensions, classifying aerosol types, and investigating the mechanisms underlying their accumulation and variation. Notably, we capitalize on CALIPSO's nighttime detection capabilities to explore aerosol behavior during periods often neglected in past studies.

This research makes several key contributions. First, it provides the first long-term, basin-specific characterization of vertical aerosol structures using satellite lidar data. Second, it enhances our understanding of aerosol layering and seasonal evolution in a closed terrain setting. Third, by identifying dominant aerosol types and their vertical distribution patterns, this work offers new insights into pollution formation mechanisms and provides scientific support for air quality regulation in basin regions. The findings also serve as a valuable reference for other topographically complex regions worldwide facing similar environmental challenges.

2. Methodology

2.1 Study Area

The Sichuan Basin (Figure 1), located in southwestern China, is one of the country's four major basins, covering an area of over 260,000 square kilometers.

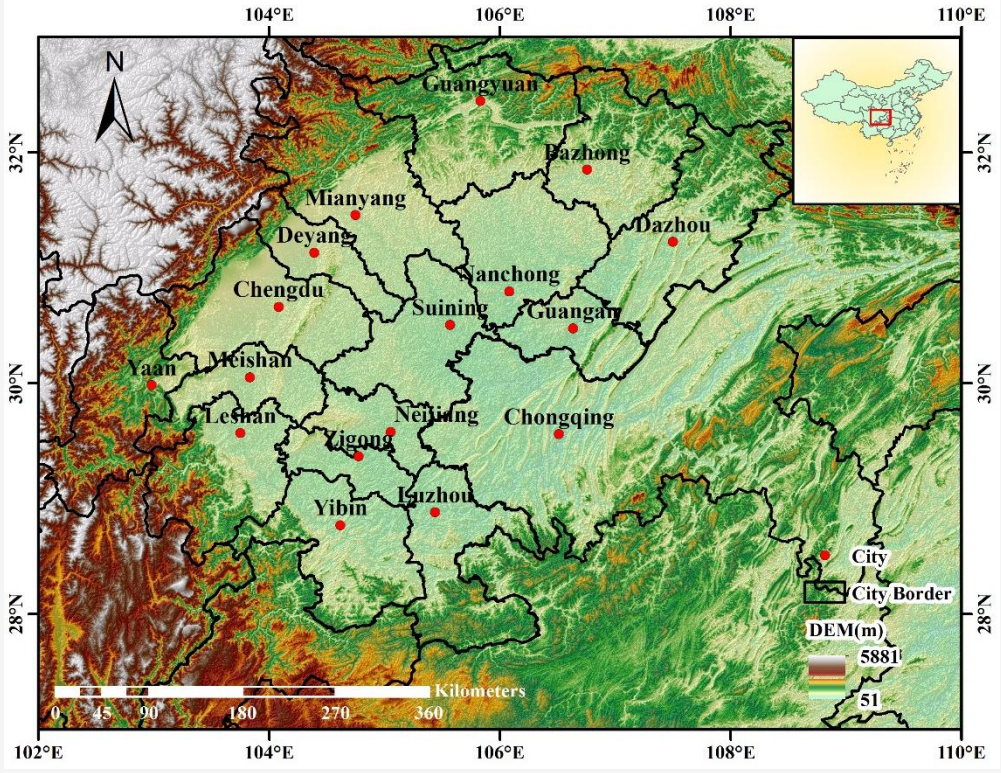

Figure 1: DEM rendering of the Sichuan Basin

It is surrounded by the Tibetan Plateau, Daba Mountains, Huaying Mountains, and Yunnan-Guizhou Plateau, with elevation differences ranging from approximately 50 meters to over 5,000 meters. The basin experiences a subtropical monsoon humid climate, characterized by temperature variations influenced by both topography and geographic location. Generally, temperatures are higher in the east than in the west, higher in the south than in the north, and warmer at the basin's bottom compared to its edges, resulting in concentric isotherm patterns. The average summer temperature ranges from 24 to 28°C, while the average winter temperature ranges from 4 to 8°C. Annual precipitation varies between 1,000 and 1,300 millimeters, with an uneven seasonal distribution. Approximately 70–75% of the total rainfall occurs between June and October [14] and [15]. The basin is home to 17 major cities, including Chengdu and Chongqing, both classified as megacities with populations exceeding 20 million. The southwestern region of the basin is more densely populated and industrially developed. Rapid social and economic development has led to widespread aerosol pollution in recent years, posing a significant environmental challenge. Chengdu, the capital of Sichuan Province, has been ranked among the most polluted cities in China, with PM2.5 concentrations significantly exceeding World Health Organization (WHO) limits. Other cities within the basin also experience similarly poor air quality [16] and [17].

2.2 Data and Method

CALIPSO is the first satellite capable of monitoring the vertical distribution of clouds and aerosols, providing global-scale data on both horizontal and vertical aerosol distributions while automatically identifying different aerosol types [7][18] and [19]. It is equipped with three primary instruments: the dual-channel (532 nm and 1064 nm) Cloud-Aerosol Lidar with Orthogonal Polarization (CALIOP), an Imaging Infrared Radiometer (IIR), and a Wide-Field-of-View Camera (WFC) [20] and [21]. The key parameters of these instruments are listed in Table 1. The CALIOP lidar collects remote sensing data both during the day and at night. NASA processes CALIPSO data into five levels of products: Level 0, Level 1A, Level 1B, Level 2, Level 3, and Level 4. Level 2 products, which include layer products, profile products, and vertical feature mask products, provide information on aerosol extinction coefficients, layer features, backscatter coefficients, color ratios, depolarization ratios, and aerosol categories [22] and [23]. In this study, CALIPSO Level 2 daytime and nighttime aerosol products from 2006 to 2023 were used. Since the CALIPSO data are laser point cloud data and visualized as a straight line, a too small resampling resolution will result in a large number of null raster cells, so the Level 2_Alay data were resampled onto a 1° × 1° latitude/longitude grid, averaging Aerosol Optical Depth (AOD) values while excluding nulls and values ≤ 0, we then analysed the general spatiotemporal distribution of AOD, the biennial spatiotemporal distribution, the seasonal spatiotemporal distribution. In terms of the vertical spatiotemporal distribution, The 532 nm total backscatter coefficient, particle depolarization ratio, and color ratio (derived from the 1064 nm and 532 nm total backscatter coefficients) in the Level 2_Apro data were averaged over the study area with a vertical resolution of 60 meters, after the analysis of times series, and In order to make the vertical distribution more intuitive and linearized, the data were stratified into 2 km height intervals, covering altitudes from 0 to 10 km within the troposphere, a height stratification analysis was implemented. The aerosol type parameter "Feature_Classification_Flags" in the Level 2_VFM data includes seven aerosol types, whose occurrence frequencies were calculated and stratified into 2 km intervals from 0 to 8 km, we finally performed an analysis of the proportion and vertical distribution of aerosol species. All aerosol characteristics above were compared between daytime and nighttime data to highlight similarities and differences. To visually present the data processing workflow, we created a flowchart (Figure 2).

3. Results and Analysis

3.1 AOD Spatiotemporal Distribution of the Sichuan Basin

AOD is a fundamental physical parameter that quantifies how aerosols attenuate light. Defined as the vertical integral of the medium's extinction coefficient, AOD indicates the degree to which aerosols reduce light transmission and serves as a key measure of atmospheric haze or turbidity. Analyzing the spatiotemporal variation of AOD across the Sichuan Basin provides a reliable basis for understanding the horizontal distribution of aerosols within the region [24] and [25].

3.1.1 AOD general spatiotemporal distribution

Figure 3 shows the spatial distribution map derived from the 18-year average of AOD values. High AOD values are concentrated in the southwestern urban areas, with the highest value of 0.63 observed in Leshan City during the day, followed by Zigong, Neijiang, and Yibin, where AOD values range from 0.5 to 0.6.

Table 1: Parameters of the CALIPSO satellite

Orbital Altitude	Runtime range	Global Coverage	Orbit Inclination
705 km (lowering in 2018)	2006-2023	82°N and 82°S	98.2°
Max. Horizontal Resolution	**Equator-crossing Time**	**Max.Vertical Resolution**	**Repeat Cycle**
333m	1:30 PM	30m	16-day

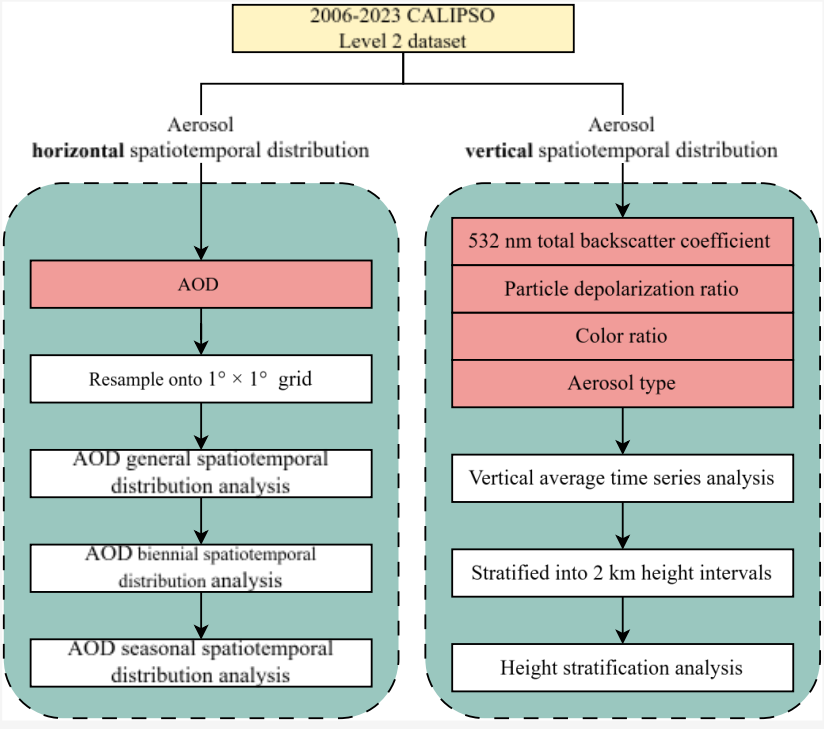

Figure 2: Flowchart of data processing

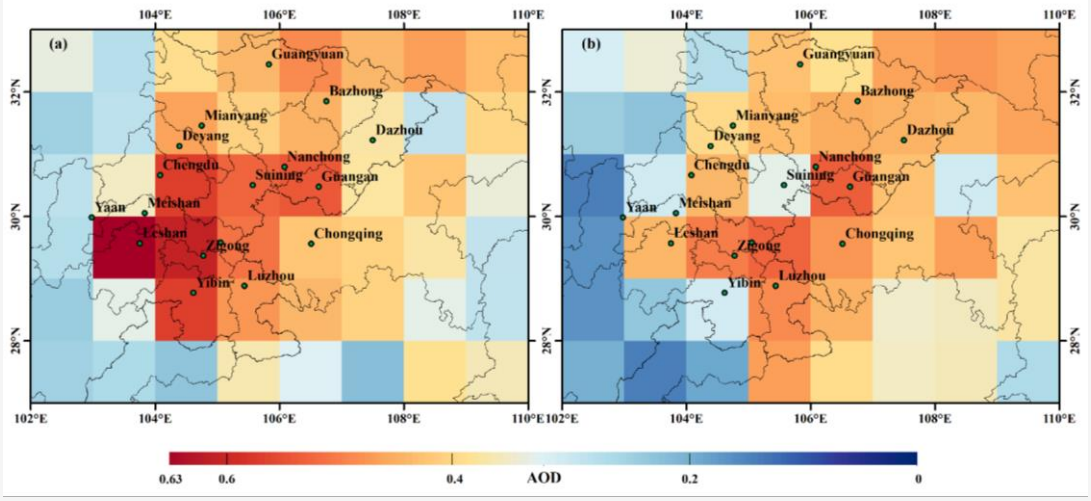

Figure 3: Spatial distribution of mean AOD in Sichuan Basin from 2006 to 2023. Green circles are city coordinates and black solid lines are city boundaries:
(a) Average AOD (daytime) 2006-2023 and (b) Average AOD (Nighttime) 2006-2023

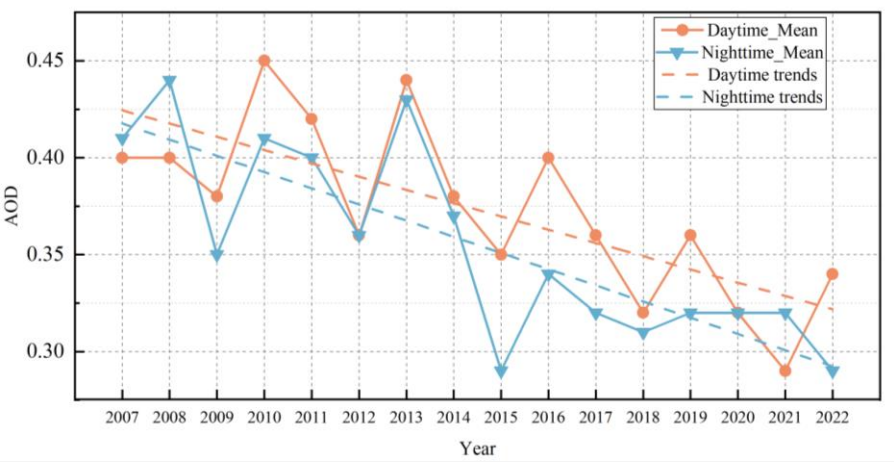

Figure 4: Trend of annual mean AOD values in the Sichuan Basin from 2007 to 2022

Nighttime AOD values are generally lower than daytime values, with the highest value of 0.52 recorded in Guang'an, followed by Zigong and Neijiang, with values around 0.45 to 0.5. Leshan, which has the highest AOD value during the day, drops to 0.45 at night. Notably, the megacities Chengdu and Chongqing do not exhibit the expected high AOD values, suggesting that AOD distribution is not solely related to population density. AOD values at the basin's outer edge are generally higher in the eastern mountainous areas compared to the west. Additionally, the lowest AOD values at the basin's outer rim are found in the southwestern mountainous areas, dominated by the Tibetan Plateau.

In summary, the AOD distribution in the Sichuan Basin generally follows a pattern of "high inside the basin, low around the basin, high during the day, and low at night." The surrounding high-altitude mountainous regions, averaging over 2,000 meters above sea level, feature thinner air and weaker atmospheric activity, effectively confining atmospheric processes within the lower basin. Cities within the basin are largely situated on the low-lying plains, with the southwestern urban agglomeration emerging as a region with high AOD values, corresponding to the area's industrial and economic development. The findings are consistent with previous studies [26][27] and [28] , further validating the observed spatial and temporal trends in AOD distribution.

To examine the temporal variation of AOD values within the basin, a linear trend analysis of the annual mean AOD values is presented in Figure 4. From 2007 to 2023 (excluding 2006 and 2023 due to incomplete data), the mean AOD value decreased from 0.4 to 0.35 during the day and from 0.4 to 0.25 at night. However, the nighttime value plateaued after 2016 before declining again in 2022. In all, the mean AOD values in the Sichuan Basin show an overall downward trend, with peaks approximately every two years. This decline is strongly correlated with the Chinese government's sustained efforts in ecological management, particularly "energy saving and emission reduction" initiatives, which have significantly impacted air quality [29] and [30].

3.1.2 AOD biennial spatiotemporal distribution

For the period from 2007 to 2022, mean values were calculated biennially, with their spatial and temporal distributions shown in Figures 5 and 6. These figures indicate that daytime and nighttime mean AOD values from 2007 to 2014 were significantly higher compared to the subsequent four years. The highest daytime AOD values occurred in the Yibin area during 2007-2008 and in the Leshan area during 2013-2014, while the highest nighttime values appeared in the Neijiang area during 2013-2014, both reaching close to 0.8. After 2013-2014, mean AOD values in urban areas within the basin decreased significantly, particularly in the southwestern urban agglomerations, where daytime AOD values remained below 0.6 and nighttime values fell below 0.5. Overall, AOD values in the basin began to decline obviously after 2014 , nighttime AOD values are generally lower than daytime values. AOD day-night difference can be attributed to weaker anthropogenic activities and reduced industrial emissions at night, as well as the characteristics of CALIOP, an active lidar system that experiences higher signal-to-noise ratios (SNR) during the day due to solar radiation influences [21] and [31].

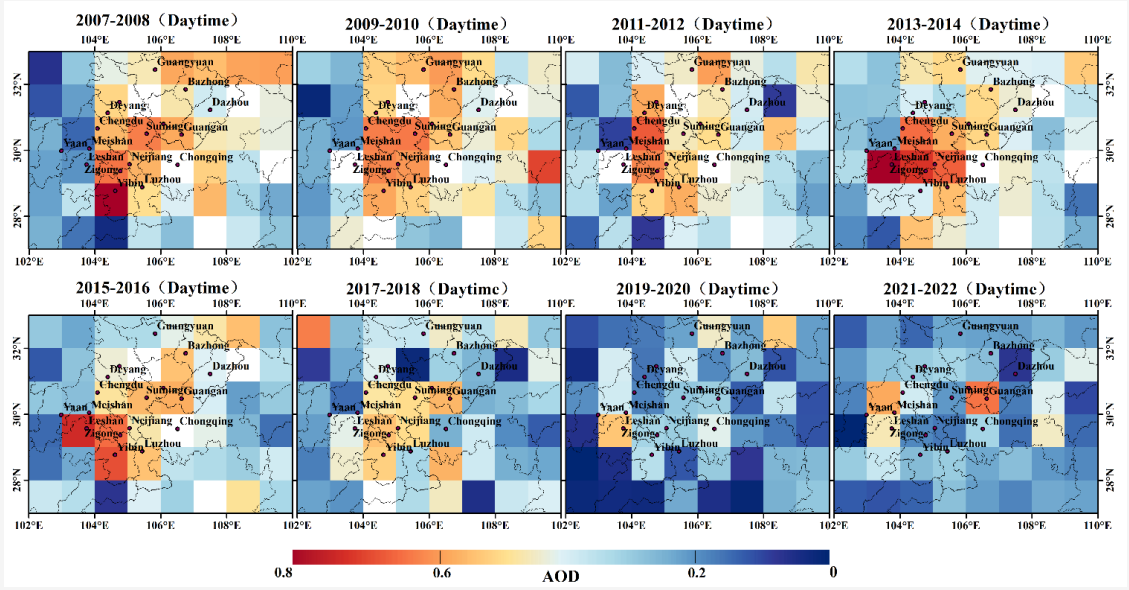

Figure 5: Spatial and temporal distribution of daytime mean AOD values in the Sichuan Basin, 2007-2023, two-year intervals

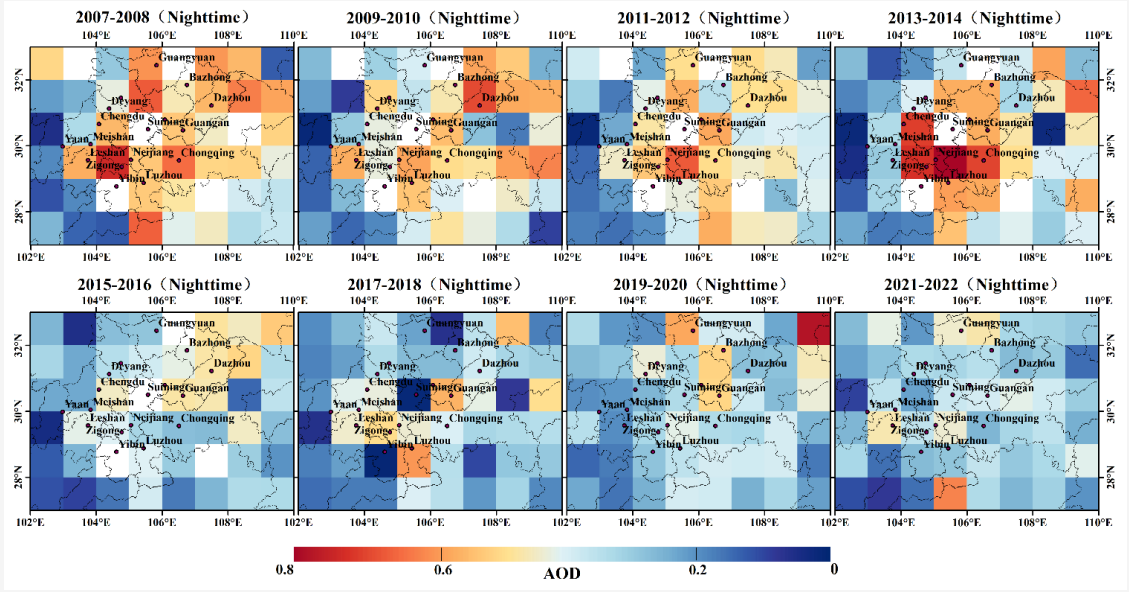

Figure 6: Spatial and temporal distribution of nighttime mean AOD values in the Sichuan Basin, 2007-2023, two-year intervals

3.1.3 AOD seasonal spatiotemporal distribution

Analysis of the monthly mean AOD values (Figure 7) reveals pronounced seasonal variations in the spatial distribution of AOD across the Sichuan Basin. AOD levels peak during summer and fall, followed by spring, with the lowest values observed in winter. Daytime AOD values exhibit a gradual increase from January, experience a sharp rise in July, reach a peak of 0.45 in August, and subsequently decline to 0.32 by December. In contrast, nighttime AOD values begin at approximately 0.27 in January, rise to a minor peak in April, peak at 0.45 in September, and then decrease to 0.3 by December. Figure 8 illustrates the seasonal spatial and temporal distribution of mean AOD values. During spring, high daytime AOD values are concentrated in Zigong, Yibin, and Leshan, ranging from 0.6 to 0.7. In the northeastern cities of the basin, AOD values range from 0.4 to 0.5, while nighttime AOD values in spring decrease by 0.1 to 0.2 compared to daytime levels.

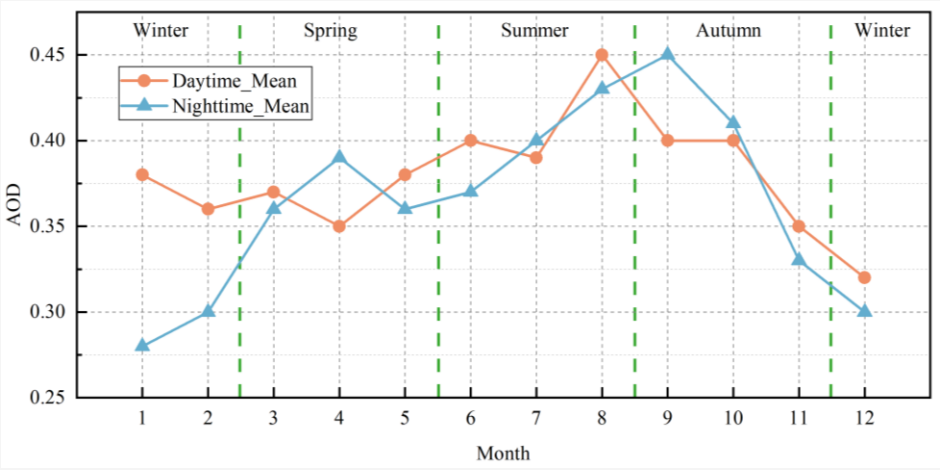

Figure 7: Monthly mean values of AOD in the Sichuan Basin. The green dashed line is the seasonal demarcation line

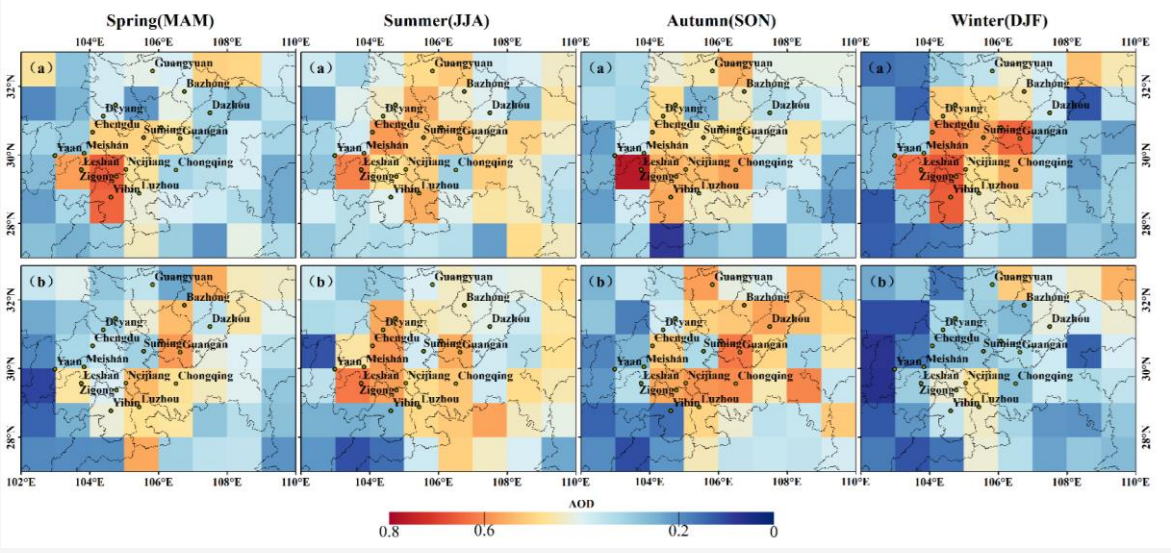

Figure 8: Seasonal spatial-temporal distribution of mean AOD values in the Sichuan Basin: (a) daytime maps and (b) nighttime maps. Spring spans from March to May (MAM), summer from June to August (JJA), autumn from September to November (SON) and winter from December to February (DJF)

In summer, AOD values generally increase relative to spring, ranging from 0.5 to 0.6, with minimal differences between day and night distributions. During fall, AOD levels remain elevated across the basin, with Leshan City approaching a daytime maximum of 0.7, while other cities exhibit values ranging from 0.5 to 0.6. In winter, AOD values in the mountainous regions along the basin's periphery drop to their lowest annual levels. Significant day-night variations are observed, with daytime peaks nearing 0.7 in Yibin, Zigong, and Leshan, while other cities maintain daytime values around 0.5. Nighttime AOD values in high-AOD regions decrease to approximately 0.5, and in other areas, they drop to 0.2–0.3. To further analyze the differences in daytime and nighttime AOD distributions, we calculated and plotted these differences on a spatio-temporal distribution map (Figure 9). The difference value in the figure represents the daytime AOD minus the nighttime AOD. The largest differences occur in winter, reaching up to 0.4, and are mainly concentrated in urban areas in the central and western parts of the basin. In autumn, Leshan and Yibin in the southwest also show a difference of 0.4, while Dazhou and Bazhong in the northeast have negative values, indicating that nighttime AOD is slightly higher than daytime AOD.

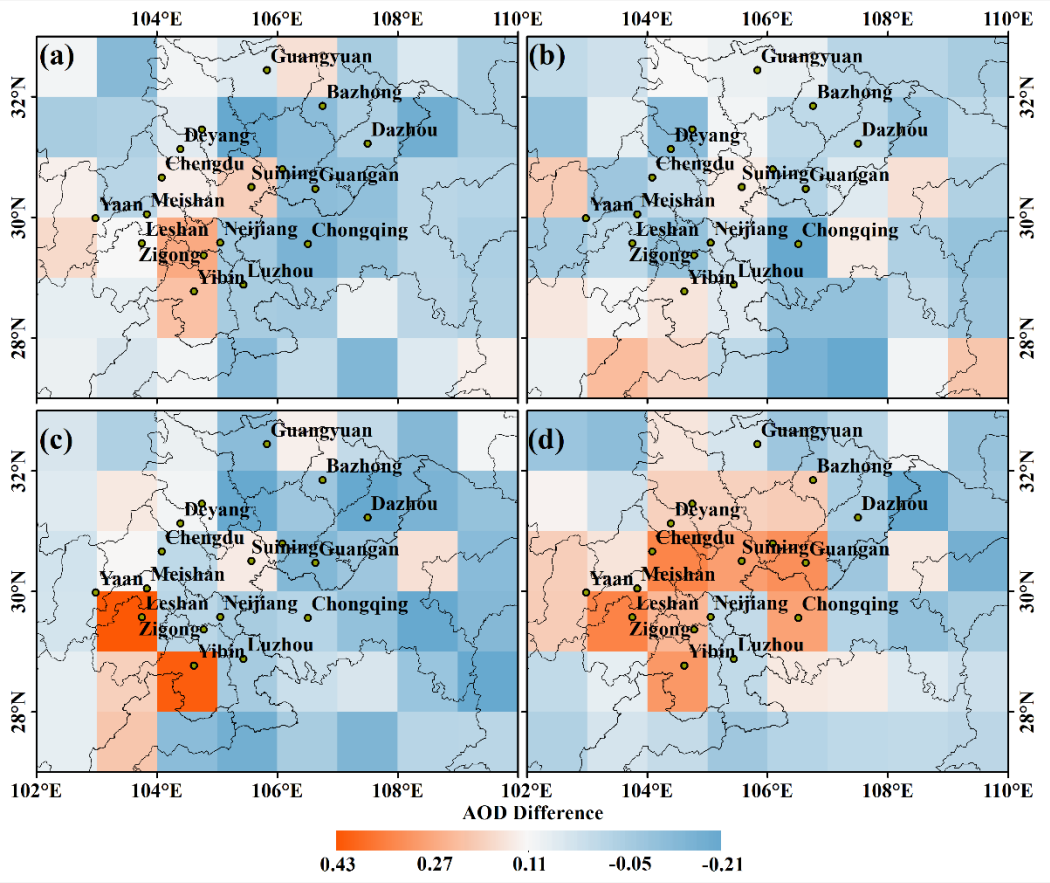

Figure 9: Difference between mean daytime and nighttime AOD:
(a) spring (MAM); (b) summer (JJA); (c) autumn (SON); (d) winter (DJF)

In summer, AOD differences are minimal, with little variation between day and night. In spring, Zigong and Yibin in the southwest continue to show significant AOD differences, while northeastern cities have negative values. However, the magnitude of these differences in spring is smaller compared to autumn and winter. In summary, seasonal changes in AOD across the Sichuan Basin showed that peak values were reached in summer and autumn, followed by spring, and the lowest in winter. However, winter conditions often lead to localized pollutant accumulation. In the southwestern urban agglomeration, AOD values can reach as high as 0.7, while some surrounding high-altitude areas may register values close to 0. The reduced atmospheric activity during winter frequently results in the formation of inversion layers over the Sichuan Basin, causing pollutants to sink and accumulate. This limited surface atmospheric flow contributes to haze formation, posing significant health risks. Notably, AOD values during winter drop dramatically at night, with differences exceeding 0.4 compared to daytime values. This suggests a significant reduction in air pollution at night, likely due to decreased anthropogenic activities and the effects of strong nighttime inversion layers leading to pollutant deposition. Further research is needed to validate these observations.

3.2 Vertical Distribution Characteristics of Aerosols in the Sichuan Basin

3.2.1 Vertical distribution of 532nm total backscatter coefficient

The total backscatter coefficient from the two 532 nm polarization channels measured by CALIPSO reflects the light scattering strength of atmospheric particles, with higher values indicating stronger scattering. The effective range of the 532 nm backscatter coefficient for aerosols is 0.003-0.009 $sr^{-1}.km^{-1}$, with a threshold value of 0.0015 $sr^{-1}.km^{-1}$ for the aerosol layer top height [32] and [33]. Vertical profiles of 532 nm backscatter coefficients for the study region were averaged into a single profile and then monthly averaged to create the 2006-2023 time series image (Figure 10).

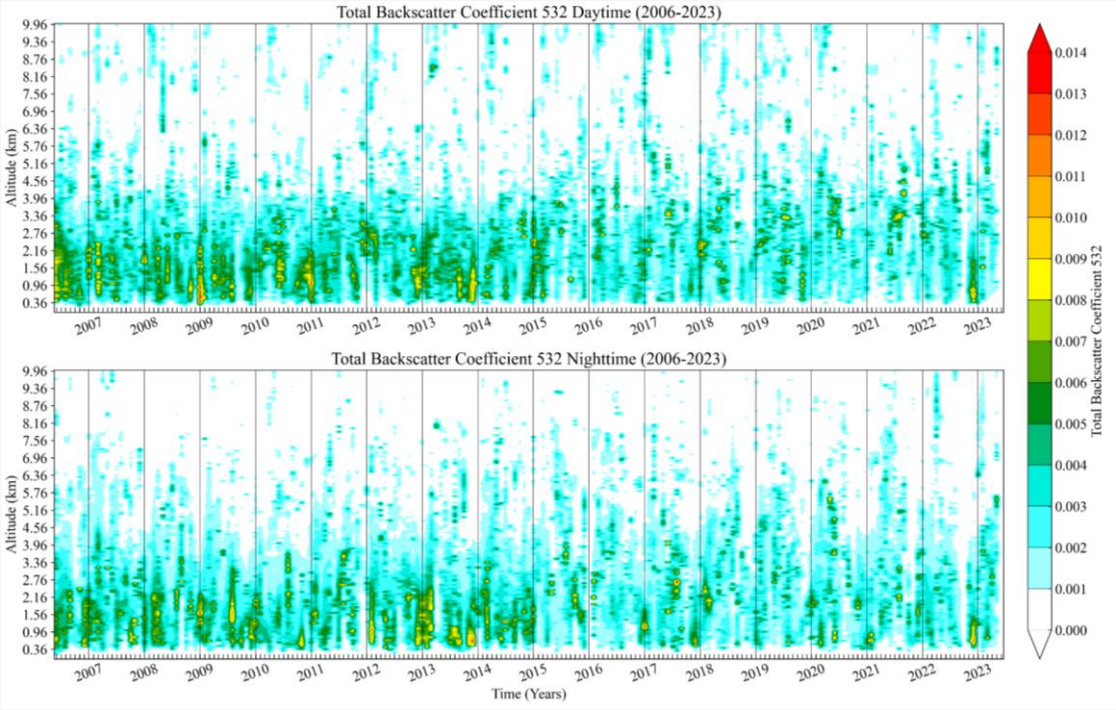

Figure 10: Time series plot of vertical profile of total backscattering coefficient at 532 nm

The backscatter coefficients primarily ranged from 0 to 0.0014 $sr^{-1}.km^{-1}$, with notable reductions after 2015. Nighttime values were consistently lower than daytime values. Vertically, the backscatter coefficient generally decreases with altitude, with higher values concentrated between 0 and 3 km. A daytime peak occurred in January 2009, exceeding 0.012 $sr^{-1}.km^{-1}$, within a vertical range of about 0 to 2.5 km. A nighttime peak was observed in November 2013, with sustained high values around 0.5 km in altitude. Figure 11 illustrates the monthly height-stratified statistics of backscatter coefficients, using a 2 km height interval. Backscatter coefficients below 4 km generally exceed 0.002 $sr^{-1}.km^{-1}$, significantly higher than those at other height levels. Within the 0-2 km range, backscatter coefficients exhibit a "W" pattern throughout the year, decreasing from January to a minimum of approximately 0.0026 $sr^{-1}.km^{-1}$ in May, forming a trough in May and June. They recover in July, decrease again in August and September, and then rapidly recover in December after reaching another trough in October and November. The backscatter coefficients at the 0-4 km range display an "M" shape annually, starting with a gradual increase from January, peaking in March and April, then dropping to a trough, peaking again in September, and finally decreasing. As altitude increases, the backscatter coefficients stabilize within a narrower range. Overall, the 532 nm backscatter coefficient in the Sichuan Basin generally decreases with height, with higher values concentrated within the 0 to 3 km range. A notable reduction in backscatter coefficients has been observed since 2015, which aligns with findings from MODIS AOD studies in the Sichuan Basin [27] and [28], this reduction is likely attributable to the implementation of China's new environmental protection law in 2015, which has contributed to environmental improvements [34].

3.2.2 Vertical distribution of color ratio

The color ratio, defined as the ratio of the backscattering coefficient at 1064 nm to that at 532 nm, indicates the particle size of atmospheric particles, with higher values corresponding to larger particle sizes[35]. Figure 12 presents the time series of the vertical profile of the color ratio in the study area, the color ratio primarily shows a point-like distribution, with values ranging from 0 to 3.8. Daytime color ratio values are significantly lower than nighttime values, and since 2014, the daytime distribution has increased, mainly below 5 km. At night, the color ratio distribution is more concentrated compared to the daytime and has been steadily increasing since 2006, predominantly at altitudes above 3 km. Figure 13 illustrates the height-stratified monthly statistics of the color ratio, with a 2 km height interval.

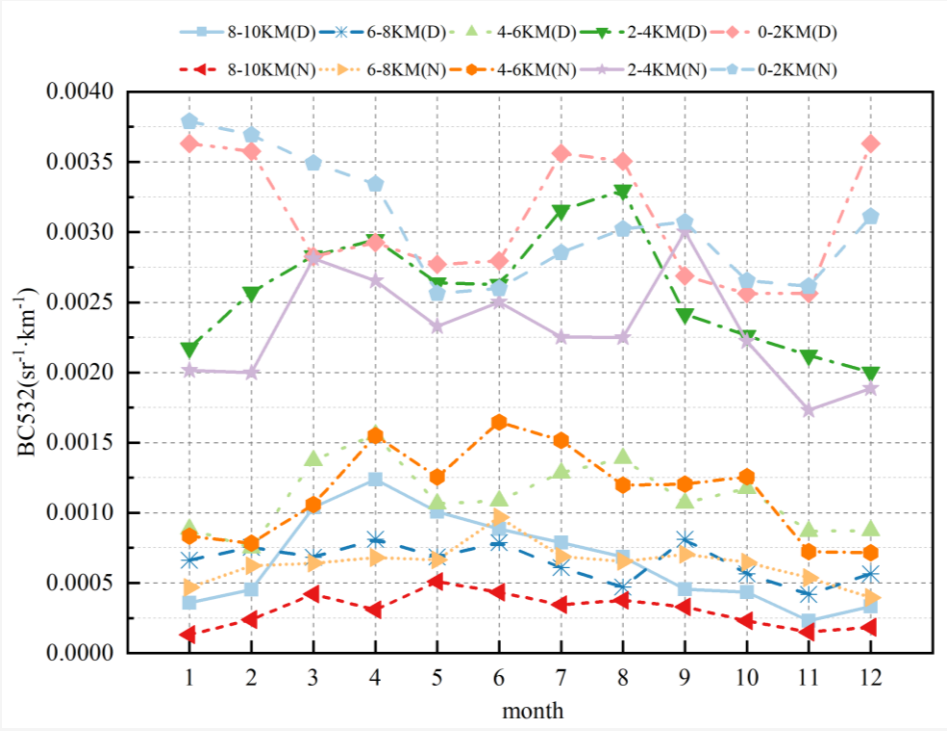

Figure 11: Monthly average statistics of 532nm total backscatter coefficient height stratification

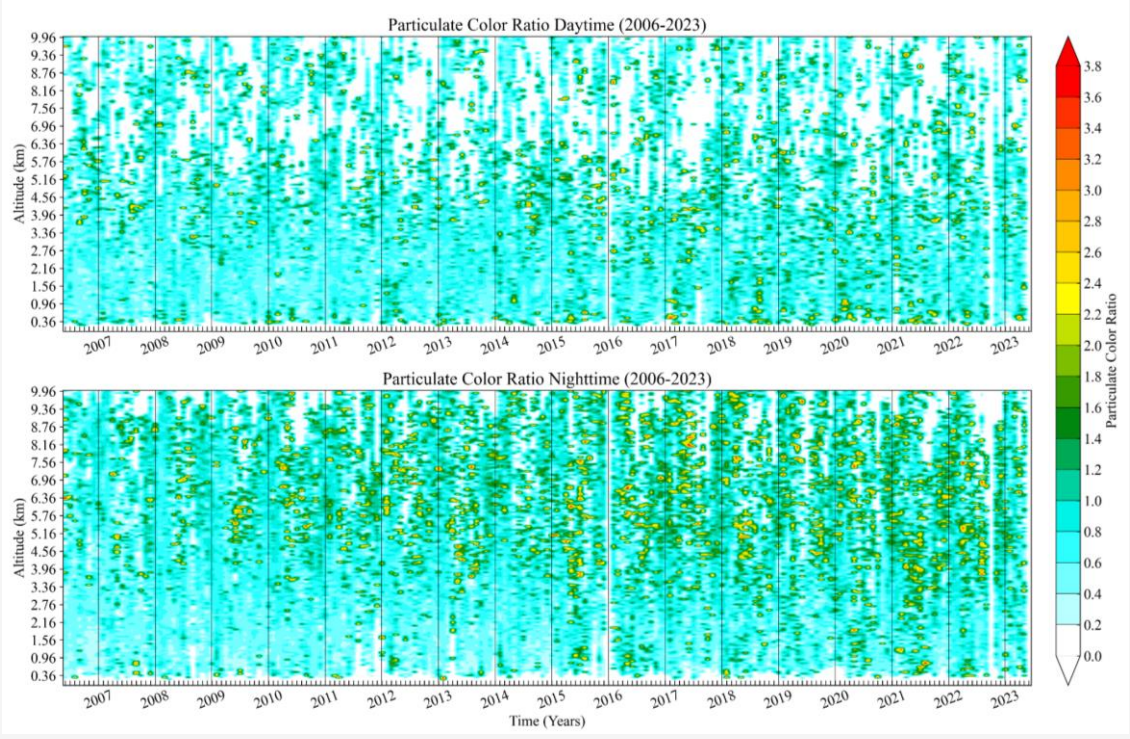

Figure 12: Time series on vertical profile of color ratio distribution

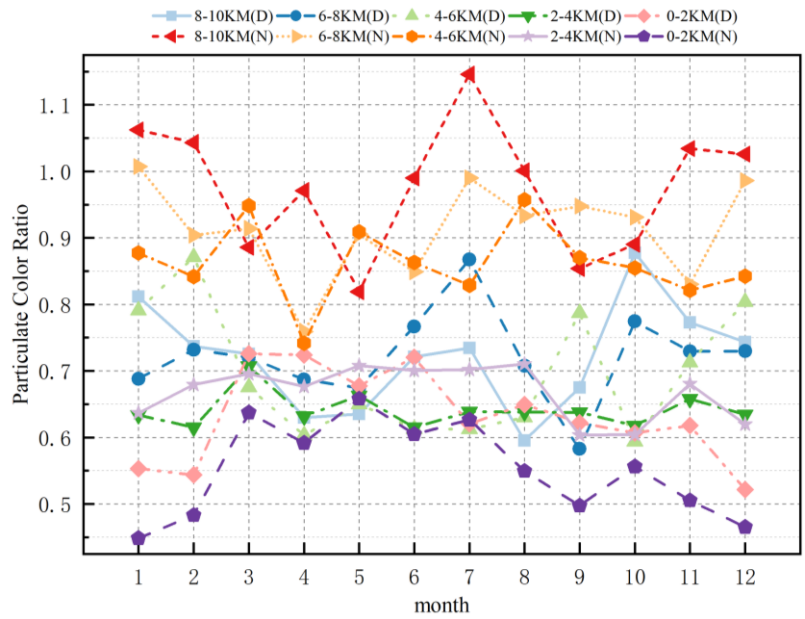

Figure 13: Monthly average statistics of color ratio height stratification

The figure 13 shows that at night, the color ratio above 4 km consistently exceeds 0.8, displaying a wavelike pattern with higher values in summer and winter, and lower values in spring and fall. At night, the color ratio between 0 and 4 km remains below 0.7, with the lowest values occurring in winter. During the daytime, the color ratio generally stays below 0.8. Above 4 km, a seasonal trend similar to nighttime is observed, while below 4 km, the values are smaller and exhibit less fluctuation.

3.2.3 Vertical distribution of 532nm depolarization ratio

The CALIOP sensor features two perpendicular 532 nm polarization channels. The ratio of their signals, known as the depolarization ratio (PDR), indicates the sphericity of atmospheric particles, with a lower ratio suggesting particles are closer to a spherical shape[36]. Figure 14 presents the time series of the PDR vertical profile in the study area from 2006 to 2023, the depolarization ratio ranges from 0 to 0.34, with higher daytime PDR values compared to nighttime. At night, the PDR exhibits more pronounced seasonal variation, with higher values in winter and spring. During the day, the PDR is concentrated between 0 and 5 km altitude, whereas at night, it is concentrated between 3 and 8 km. Peaks in the PDR observed in January and February 2012 suggest an increased presence of irregular aerosol particles during this period. Additionally, the nighttime PDR from October to March is higher, with the duration of elevated PDR being the longest among all years. Figure 15 illustrates the height-stratified statistics of the PDR with a 2 km interval. Except for a rebound in the 0-4 km range during the daytime from June to September, the overall trend in the stratified distribution of the PDR shows an upward trend beginning in October, peaking in April, and then declining in summer, forming a trough from July to September, likely due to increased humidity during the rainy season. During the daytime, the PDR is higher at 0-4 km, mostly above 0.8, while it drops below 0.8 above 4 km. The 6-8 km range has the lowest PDR, with a minimum value close to 0.02 in October. At night, the PDR is highest between 2-6 km, reaching up to 0.15 at 4-6 km. The PDR is lower at 0-2 km, with the lowest value around 0.03 at 6-8 km in July and August.

Combining vertical observations of the color ratio, it is inferred that irregular large particles are predominantly concentrated below 5 km during the day. At night, these particles ascend to heights of 3 to 8 km, a phenomenon likely influenced by the basin's unique topography. The significant temperature difference between the valley floor and the surrounding mountainous areas at night drives thermal circulation. During the day, the prevalence of sinking airflow inhibits the formation of precipitation. In contrast, at night, the higher temperatures of the valley floor promote updrafts, facilitating the ascent of irregular large aerosol particles [37][38] and [39]. This process enhances water vapor condensation and the formation of precipitation.

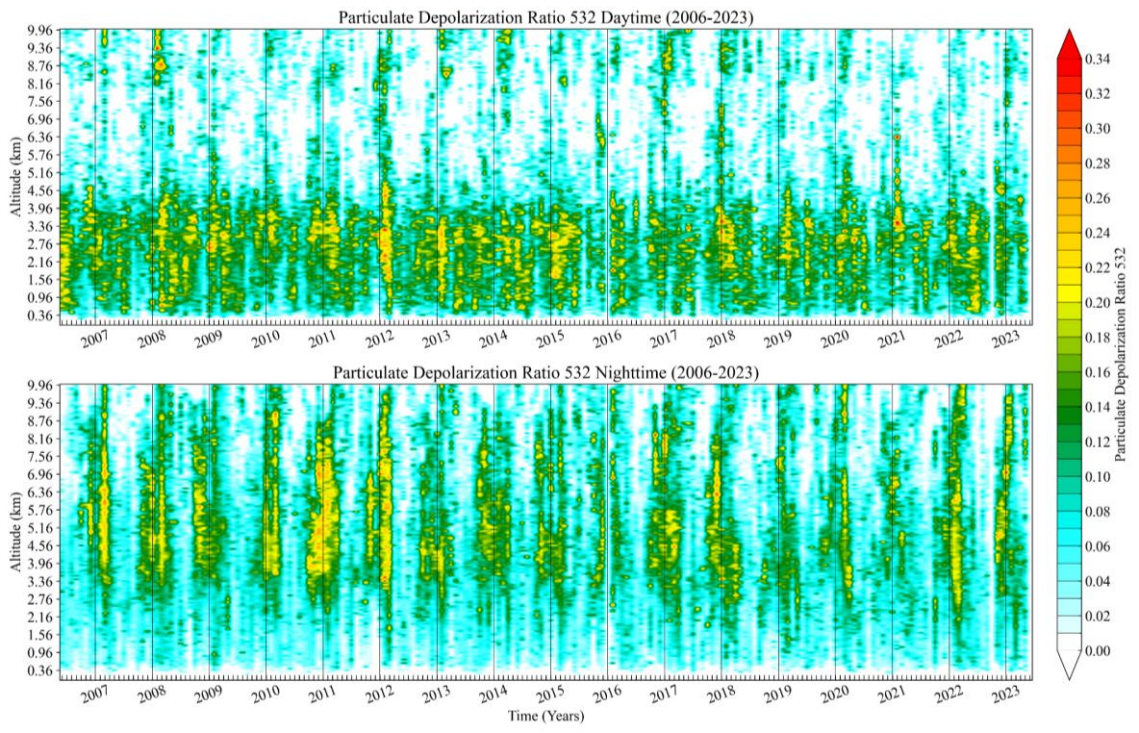

Figure 14: Time series for vertical profiles of particle depolarization ratio

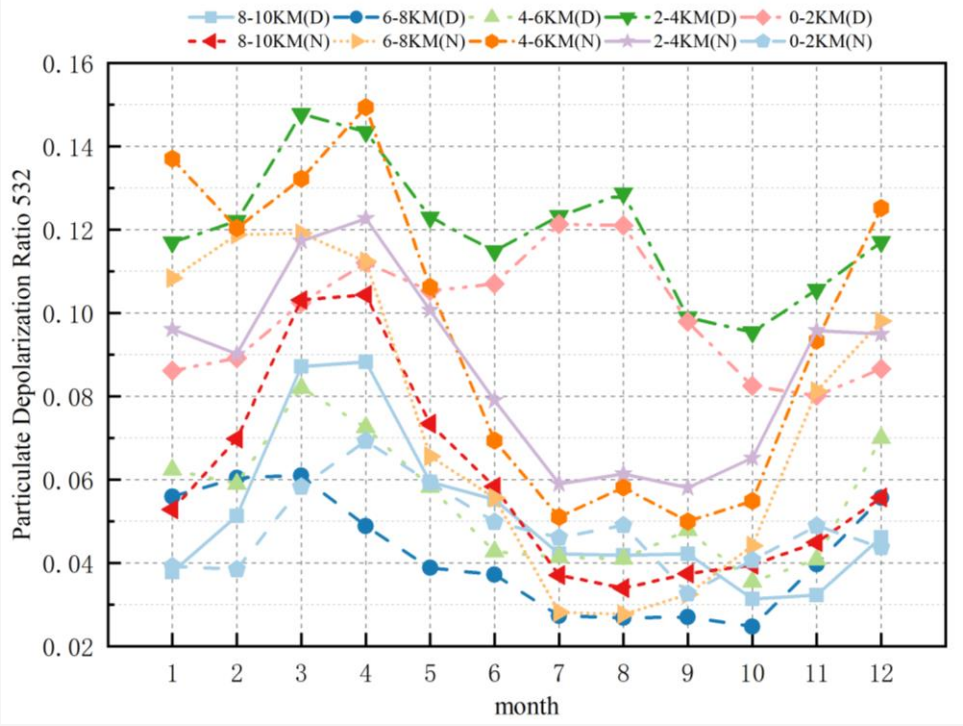

Figure 15: Monthly average statistics of particle depolarization ratio height stratification

Table 2: Aerosol species classified by the CALIPSO satellite

Category	Abbreviation	Description
Clean Marine	CM	Mainly composed of marine droplets, including sea salt, organic matter, and small amounts of sulfate.
Dust	Du	Primarily originating from natural sources like sand and dust.
Smoke	Sm	A mixture of soot, sulfides, and other compounds, mainly from biomass combustion.
Clean Continental	CC	Represents clean, naturally occurring continental aerosols.
Polluted Dust	PD	A secondary polluted aerosol, primarily of the dust type.
Elevated Smoke	ES	Smoke particles suspended at higher altitudes, usually above the boundary layer.
Dusty Marine	DM	A mixture of dust particles and marine aerosols.

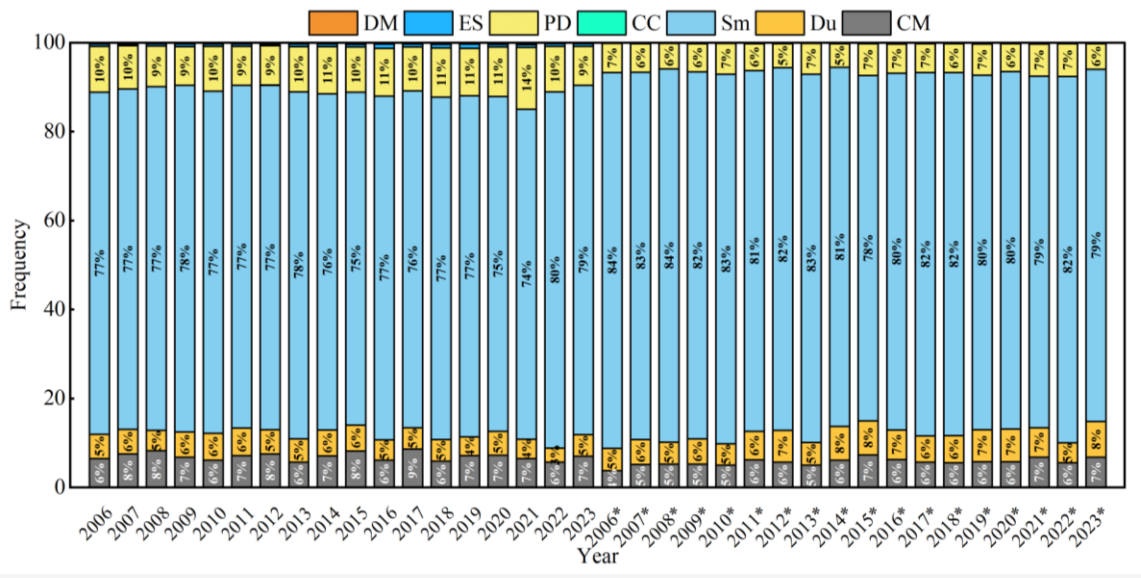

Figure 16: Annual average change in aerosol species share. *Represents nighttime data

3.2.4 Aerosol categories in the troposphere

The CALIPSO satellite classifies observed tropospheric aerosols into 7 categories as shown in Table 2. Figure 16 illustrates the annual variation in the percentage of these aerosol species in the study area. The results indicate that tropospheric aerosols in the basin are predominantly Sm, accounting for 70-80% of all aerosol species. PD follows, making up about 10%, while CM and Du each constitute around 6-7%. Notably, CC is almost negligible, and both ES and DM represent less than 2%, making them statistically insignificant in the diagram. Monthly counts of aerosol species, as shown in Figure 17, reveal that Sm consistently ranges between 74% and 79% during the daytime, with peaks in April, July, and August. At night, the proportion of Sm ranges from 79% to 85%, with the highest values in April. PD accounts for 9-12% of the total during the daytime, peaking in October and December, while at night, PD ranges from 4-8%, with peaks in July and October. Figure 18 illustrates the seasonal averages of aerosol species. The data indicates that PD is slightly lower in winter and spring compared to summer and fall. Du shows a noticeable increase in winter, being about 2 percentage points higher than in other seasons, while Sm is slightly reduced in winter compared to other seasons. Overall, the aerosol types in the Sichuan Basin mainly include Sm, PD, Du, and CM, the proportions of these aerosol species have remained stable with no significant fluctuations.

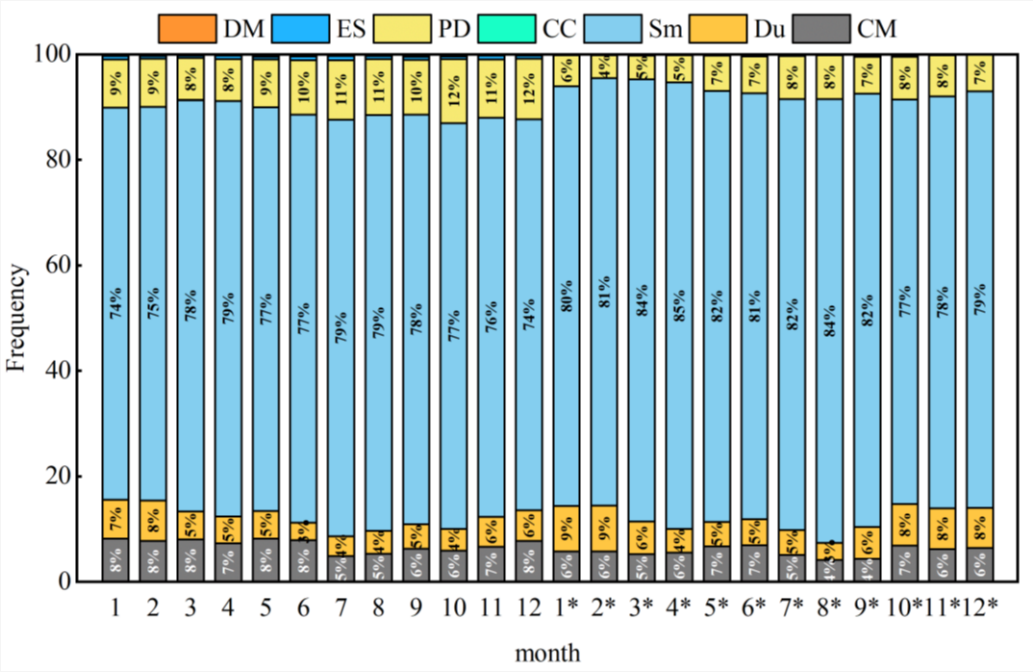

Figure 17: Monthly average statistics of aerosol types. *Represents nighttime data

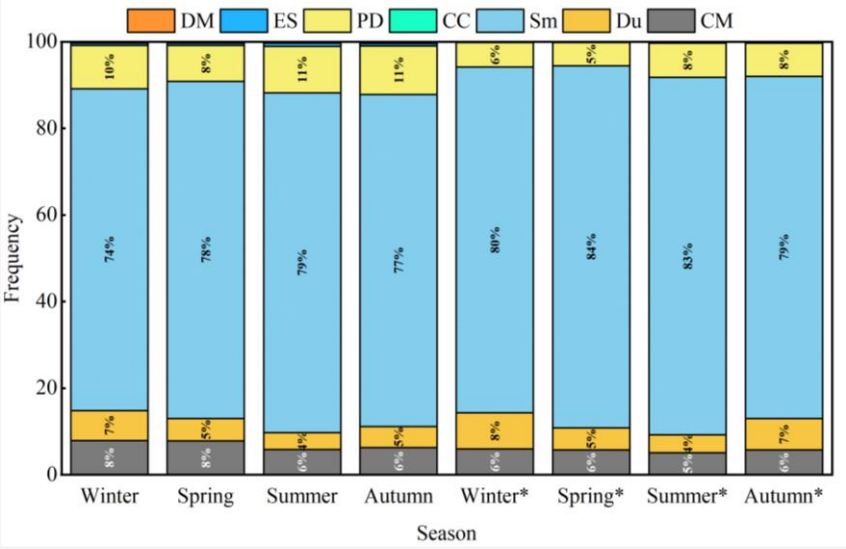

Figure 18: Seasonal statistics of aerosol species ratio. *Represents nighttime data

3.2.5 Aerosol categories vertical distribution

Aerosol species were analyzed at 2 km altitude intervals, producing the results shown in Figure 19. During the daytime, at altitudes of 6-8 km, Sm constituted 58% of the aerosols, followed by CM at 35% and Du at 7%. However, this layer accounted for only 2% of the total daytime aerosol counts. At 4-6 km, although the total aerosol count was still low, representing 10% of the daytime total, the proportion of Sm increased significantly to 78%, while CM decreased to 15%.

The 2-4 km layer contributed 46% of the daytime total, with Sm making up 82% of the aerosols, along with 3% PD, 8% Du, and 7% CM. The 0-2 km layer accounted for 42% of the daytime total, where PD constituted 20%, and Sm maintained a 74% share. At night, there is a notable increase in the aerosol share in the upper layers, with Sm remaining the dominant aerosol species. Similar to the daytime, the proportion of PD increases at lower altitudes, with PD accounting for 23% in the 0-2 km layer.

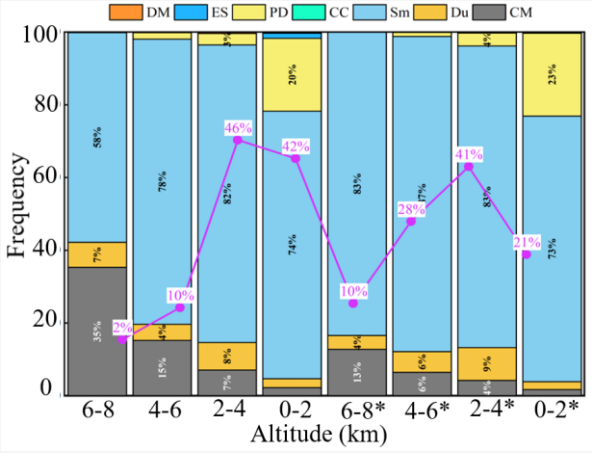

Figure 19: illustrates the vertical distribution statistics of aerosol species. The purple line represents the proportion of the aerosol number relative to the total for each corresponding altitude layer.
* represents nighttime data

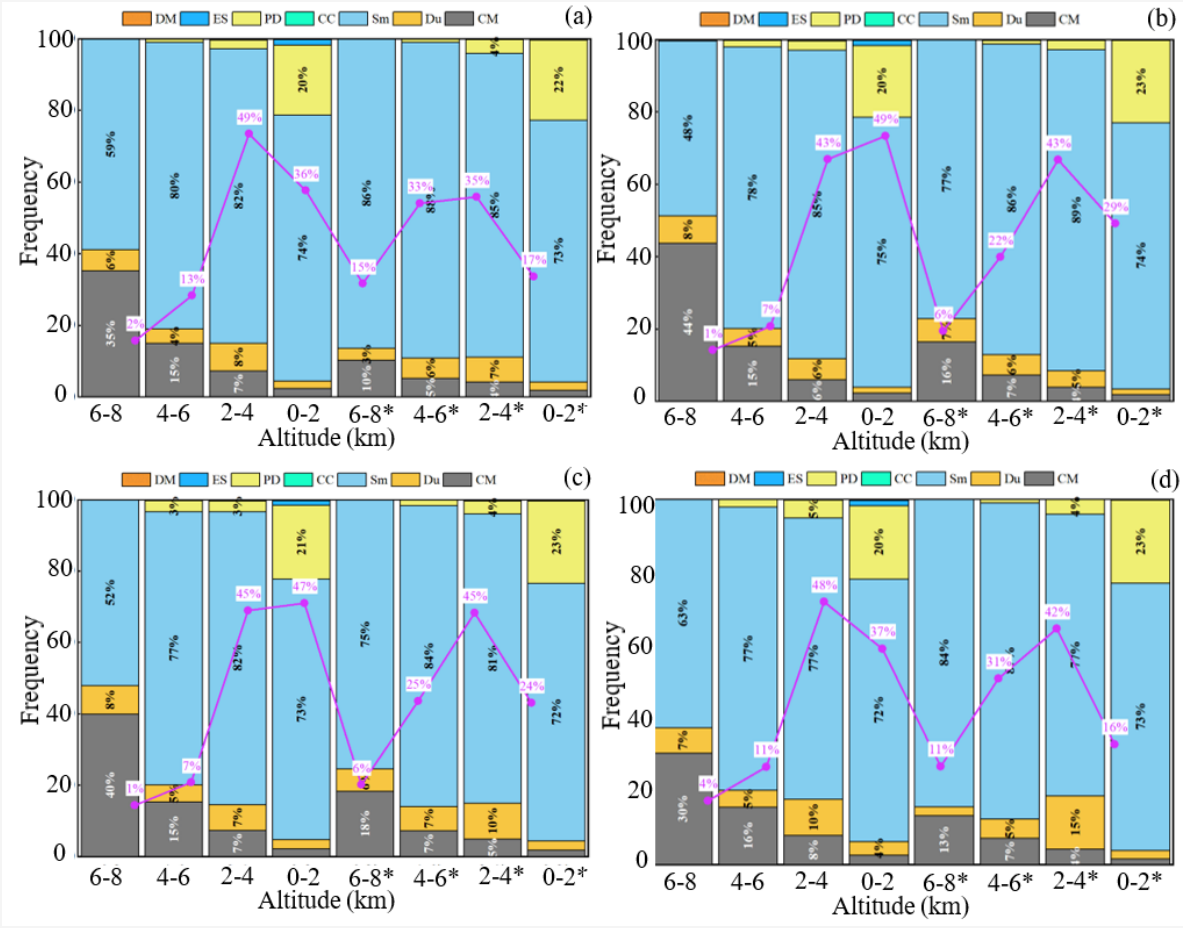

Figure 20: Seasonal vertical distribution statistics of aerosol species. The purple line is the proportion of the aerosol number in the total for the corresponding altitude layer:
(a) Spring (MAM), (b) Summer (JJA), (c) Autumn (SON), (d) Winter (DJF); * represents nighttime data

However, in terms of the total number of aerosols, the share of 0-2 km decreased from 42% during the day to 21%. Figure 20 illustrates the seasonal statistics of the vertical distribution of aerosol species. It shows that the proportion of each aerosol species within the same altitude layer remains relatively consistent across different seasons. The overall pattern of the percentage bar graph indicates minimal change, suggesting a stable distribution pattern. The proportion of aerosol quantities at various altitude layers relative to the total aerosol count forms an "M" shape. This indicates that aerosol quantities in the upper layers, both during the daytime and nighttime, are smaller compared to those in the lower layers. During the summer and autumn, the aerosol content within the 0-2 km layer during the daytime is the highest, approaching 50%. In contrast, during the winter and spring, the proportion of aerosols within the 2-4 km layer exceeds that of the 0-2 km layer, also nearing 50%. Regardless of the season, nighttime observations reveal an increase in aerosol height, with a significant rise in aerosol quantities in the 4-8 km altitude range.

All in all, the vertical spatial and temporal distribution of aerosol types suggests that aerosols in the Sichuan Basin primarily originate from biomass fuel combustion, closely linked to human activities and industrial development. This finding is consistent with the horizontal distribution of AOD, where the stability of aerosol type ratios indicates a high presence of endogenous aerosols in the basin [33]. This aligns with the stable atmospheric environment observed in the Sichuan Basin.

4. Conclusion

This study systematically analyzed the spatiotemporal characteristics of AOD and vertical aerosol properties in the Sichuan Basin using CALIOP data. The results reveal a distinct AOD pattern of “high inside the basin, low around the basin,” with higher values occurring during the day and lower values at night. The unique topographical structure of the basin surrounded by high-altitude mountains plays a significant role in confining aerosols and modulating atmospheric circulation. Southwestern urban agglomerations, as industrial and economic hubs, consistently exhibited elevated AOD levels.

Over the past decade, mean AOD values in the region have shown a clear downward trend, particularly since 2014, with fluctuations occurring approximately every two years. This trend strongly correlates with national ecological governance policies, especially energy-saving and emission-reduction initiatives, and the implementation of environmental protection laws. Vertical analysis based on CALIOP data indicates that aerosol concentrations are mainly confined to the 0–3 km layer, with notable decreases in the 532 nm backscatter coefficient after 2015, further confirming the positive effects of emission control policies.

Day-night and seasonal variations in AOD are also pronounced. Daytime AOD values exceed nighttime levels due to reduced anthropogenic emissions and stronger atmospheric stability at night. Seasonally, AOD peaks during summer and autumn but drops significantly in winter, although stable atmospheric layers during cold seasons often lead to localized pollutant accumulation and haze formation. Vertical observations suggest that large, irregular aerosol particles rise to higher altitudes at night, likely driven by thermal circulations specific to the basin's terrain.

Furthermore, aerosol type classification shows a predominance of Sm, PD, Du, and CM aerosols, with their relative proportions remaining stable. This suggests a high concentration of endogenous aerosols, primarily originating from biomass burning and industrial activities. Overall, this research not only enhances the understanding of aerosol dynamics in complex terrain regions like the Sichuan Basin but also highlights the significant impact of anthropogenic activities and policy interventions on air quality. The findings of the study can be used as a reference for government departments to carry out targeted air pollution management in response to the distribution of high AOD values at different periods of time.

5. Limitations and Future Research

In this study, we have explored various aspects of aerosols in the Sichuan Basin, but there are still some limitations: the LiDAR data of CALIPSO are point data, the spatial coverage is too small, and there are many differences with other remote sensing means, and we can consider integrating multi-source remote sensing data, such as ground-based observation data and satellite passive remote sensing data, to increase the data coverage, so as to improve the 3D spatial and temporal distribution of aerosol statistical accuracy, or multi-source data to compare and validate the data accuracy of CALIPSO. Furthermore, this study presents a preliminary discussion and analysis of the factors influencing the three-dimensional spatiotemporal distribution of aerosols. Future research should focus on quantitatively investigate the driving factors behind these distributions within the Sichuan Basin.

Such investigations could include analyses of meteorological conditions, industrial and anthropogenic sources and regional climate patterns such as temperature, wind speed, rainfall, pollutant emissions, gross regional product (GRP), gross industrial product (GIP), and the extent of human activity to better understand their impact on aerosol distribution.

Acknowledgement
Appreciation to NASA and the Centre National d'Etudes Spatiale (CNES) for the construction and maintenance of the CALIPSO satellite and for the public release of the data.

Reference

[1] Chen, Y., Xie, S., Luo, B. and Zhai, C., (2014). Characteristics and Origins of Carbonaceous Aerosol in the Sichuan Basin, *China*. *Atmospheric Environment*, Vol. 94, 215-223. https://doi.org/10.1016/j.atmosenv.2014.05.037.

[2] Barnaba, F. and Gobbi, G. P., (2004). Aerosol Seasonal Variability Over the Mediterranean Region and Relative Impact of Maritime, Continental and Saharan Dust Particles Over the Basin from MODIS Data in the Year 2001. *Atmospheric Chemistry and Physics*, Vol. 4, 2367-2391. https://doi.org/10.5194/acp-4-2367-2004.

[3] Tripathi, S. N., Dey, S., Chandel, A., Srivastava, S., Singh, R. P. and Holben, B. N., (2005). Comparison of MODIS and AERONET Derived Aerosol Optical Depth Over the Ganga Basin, India. *Annales Geophysicae*, Vol. 23,1093-1101. https://doi.org/10.5194/angeo-23-1093-2005.

[4] Papadimas, C. D., Hatzianastassiou, N., Mihalopoulos, N., Querol, X. and Vardavas, I., (2008). Spatial and Temporal Variability in Aerosol Properties Over the Mediterranean Basin Based on 6-Year (2000–2006) MODIS Data. *Journal of Geophysical Research: Atmospheres*, Vol. 113. https://doi.org/10.1029/2007JD009189.

[5] Wang, R. and Cai, H., (2023). City-Scale Aerosol Loading Changes in the Sichuan Basin from 2001 to 2020 as Revealed by MODIS 1 km Aerosol Product. *Atmosphere*, Vol. 14. https://doi.org/10.3390/atmos14121715.

[6] Winker, D. M., Pelon, J., Coakley, J. A., Ackerman, S. A., Charlson, R. J., Colarco, P. R., Flamant, P., Fu, Q., Hoff, R. M., Kittaka, C., Kubar, T. L., Treut, H. L., McCormick, M. P., Mégie, G., Poole, L., Powell, K., Trepte, C., Vaughan, M. A. and Wielicki, B. A., (2010). The CALIPSO Mission: A Global 3D View of Aerosols and Clouds. *Bulletin of the American Meteorological Society*, Vol. 91, 1211-1230. https://doi.org/10.1175/2010BAMS3009.1.

[7] Winker, D. M., Vaughan, M. A., Omar, A., Hu, Y., Powell, K. A., Liu, Z., Hunt, W. H. and Young, S. A., (2009). Overview of the CALIPSO Mission and CALIOP Data Processing Algorithms. *Journal of Atmospheric and Oceanic Technology*, Vol. 26, 2310-2323. https://doi.org/10.1175/2009JTECHA1281.1.

[8] Hu, C., Zhang, R., Lim, H. S., Zhang, Y. and Du, H., (2024). Knowledge Mapping of Cloud-Aerosol LIDAR and Infrared Pathfinder Satellite Observations Aerosol Research: A Visual Analysis Using CiteSpace. *Ocean-Land-Atmosphere Research*, Vol. 3. https://doi.org/10.34133/olar.0074.

[9] Tian, P., Cao, X., Zhang, L., Sun, N., Sun, L., Logan, T., Shi, J., Wang, Y., Ji, Y., Lin, Y., Huang, Z., Zhou, T., Shi, Y. and Zhang, R., (2017). Aerosol Vertical Distribution and Optical Properties Over China from Long-Term Satellite and Ground-Based Remote Sensing. *Atmospheric Chemistry and Physics*, Vol. 17, 2509-2523. https://doi.org/10.5194/acp-17-2509-2017.

[10] Chen, X., Yang, T., Wang, H., Wang, F. and Wang, Z., (2023). Variations and Drivers of Aerosol Vertical Characterization After Clean Air Policy in China Based on 7-Years Consecutive Observations. *Journal of Environmental Sciences.* Vol. 125, 499-512. https://doi.org/10.1016/j.jes.2022.02.036.

[11] Ma, X., Huang, Z., Qi, S., Huang, J., Zhang, S., Dong, Q. and Wang, X., (2020). Ten-Year Global Particulate Mass Concentration Derived from Space-Borne CALIPSO Lidar Observations. *Science of the Total Environment*, Vol. 721. https://doi.org/10.1016/j.scitotenv.2020.137699.

[12] Liao, T., Gui, K., Li, Y., Wang, X. and Sun, Y., (2021). Seasonal Distribution and Vertical Structure of Different Types of Aerosols in Southwest China Observed From CALIOP. *Atmospheric Environment*, Vol. 246. https://doi.org/10.1016/j.atmosenv.2020.118145.

[13] Wang, M., Hu, C., Zhao, F. Y., Wang, J. and Pan, H. L., (2021). Analysis of Stratospheric Aerosol Optical Properties in Southwest China From 2007 to 2018 Based on CALIPSO Satellite Observations. *Desert and Oasis Meteorology*, Vol. 15, 93-100.

[14] Li, X., Hussain, S. A., Sobri, S. and Said, M. S., (2021). Overviewing the Air Quality Models on Air Pollution in Sichuan Basin, *China*. *Chemosphere*. Vol. 271. https://doi.org/10.1016/j.chemosphere.2020.129502.

[15] Zhang, L., Guo, X., Zhao, T., Gong, S., Xu, X., Li, Y., Luo, L., Gui, K., Wang, H., Zheng, Y. and Yin, X., (2019). A Modelling Study of the Terrain Effects on Haze Pollution in the Sichuan Basin. *Atmospheric Environment*, Vol. 196,77-85. https://doi.org/10.1016/j.atmosenv.2018.10.007.

[16] Fang, C., Tan, X., Zhong, Y. and Wang, J., (2021). Research on the Temporal and Spatial Characteristics of Air Pollutants in Sichuan Basin. *Atmosphere*, Vol. 12. https://doi.org/10.3390/atmos12111504.

[17] Ning, G., Wang, S., Ma, M., Ni, C., Shang, Z., Wang, J. and Li, J., (2018). Characteristics of Air Pollution in Different Zones of Sichuan Basin, China. *Science of the Total Environment*, Vol. 612, 975-984. https://doi.org/10.1016/j.scitotenv.2017.08.205.

[18] Hunt, W. H., Winker, D. M., Vaughan, M. A., Powell, K. A., Lucker, P. L. and Weimer, C., (2009). CALIPSO Lidar Description and Performance Assessment. *Journal of Atmospheric and Oceanic Technology*. Vol. 26,1214-1228. https://doi.org/10.1175/2009JTECHA1223.1.

[19] Vaughan, M. A., Young, S. A., Winker, D. M., Powell, K. A. and Hostetler, C. A., (2004). Fully Automated Analysis of Space-Based Lidar Data: An Overview of the CALIPSO Retrieval Algorithms and Data Products. *Proc. SPIE 5575, Laser Radar Techniques for Atmospheric Sensing*. https://doi.org/10.1117/12.572024.

[20] Kou, L., Gao, H., Lin, Z., Li, S., Dong, P., Zhu, W., Jian, S. and Hu, X., (2023). Status and Prospect of Cloud Measurement by Satellite Active Remote Sensing. *Journal of Remote Sensing*, Vol. 27, 2041-2059. https://doi.org/10/gtp7fh.

[21] Winker, D. M., Hunt, W. H. and McGill, M. J., (2007). Initial Performance Assessment of CALIOP. *Geophysical Research Letters*, Vol. 34. https://doi.org/10.1029/2007GL030135.

[22] Kim, M. H., Omar, A., Tackett, J. L., Vaughan, M. A., Winker, D. M., Trepte, C. R., Hu, Y., Liu, Z., Poole, L. R., Pitts, M. C., Kar, J. and Magill, B., (2018). The CALIPSO Version 4 Automated Aerosol Classification and Lidar Ratio Selection Algorithm. *Atmospheric Measurement Techniques*, Vol. 11, 6107-6135. https://doi.org/10.5194/amt-11-6107-2018

[23] Young, S. A., Vaughan, M. A., Garnier, A., Garnier, A., Tackett, J. L., Lambeth, J. D. and Powell, K. A., (2018). Extinction and Optical Depth Retrievals for CALIPSO's Version 4 Data Release. *Atmospheric Measurement Techniques*, Vol. 11, 5701-5727. https://doi.org/10.5194/amt-11-5701-2018.

[24] Zhang, F., (2024). Factors Influencing the Spatio–Temporal Variability of Aerosol Optical Depth Over the Arid Region of Northwest China. *Atmosphere*, Vol. 15. https://doi.org/10.3390/atmos15010054.

[25] Yuan, J., Wang, X., Feng, Z., Zhang, Y. and Yu, M., (2023). Spatiotemporal Variations of Aerosol Optical Depth and the Spatial Heterogeneity Relationship of Potential Factors Based on the Multi-Scale Geographically Weighted Regression Model in Chinese National-Level Urban Agglomerations. *Remote Sensing*, Vol. 15. https://doi.org/10.3390/rs15184613.

[26] Zhang, J. Y., Lu, X. N., Hong, J. and Meng, C. Z., (2016). Quantitative Study on the Spatiotemporal Pattern of Aerosols and their Driving Factors in Sichuan Province from 2000 to 2014. *Journal of Natural Resources*, Vol. 31,1514-1525.

[27] Wang, A. Y., Kang, P., Zhang, Y., Zeng, S. L., Zhang, X. L., Shi, J., Liu, Z. H., Xiang, W. G., Wang, K. K., Zhang, S. Y. and Lu, J. C., (2022). Spatial Differentiation and Driving Factors of Aerosol Optical Depth in Sichuan Basin from 2003 to 2018. *China Environmental Science*, Vol. 42,528-538. https://doi.org/10.19674/j.cnki.issn1000-6923.20211012.009.

[28] Wang, C. Y., He, M. Q., Chen, J. H. and Liu, Z. H., (2020). Spatiotemporal Variation Characteristics of MODIS Aerosol Optical Depth in Sichuan Basin from 2006 to 2017. *Research of Environmental Sciences*, Vol. 33,54-62.

[29] Zhang, C., (2023). Green Mountains and Clear Waters in Sichuan: New Exploration of Carbon Neutrality in the "Land of Abundance" A Review of the Report on Sichuan Province's Energy Conservation and Emission Reduction Work in 2022. *Democracy and Legal System Construction.* 10-11.

[30] 2023 Report on the State of Ecological Environment in Sichuan Province, (2023). https://sthjt.sc.gov.cn/sthjt/c104157/2024/6/5/616637e7664946f0baf243d359985737.shtml.

[31] Powell, K. A., Hostetler, C. A., Vaughan, M. A., Lee, K. P., Trepte, C. R., Rogers, R. R., Winker, D. M., Trepte, C. R., Liu, Z., Rogers, R. R., Kuehn, R., Hunt, W. H. and Young, S. A., (2009). CALIPSO Lidar Calibration Algorithms. Part I: Nighttime 532-nm Parallel Channel and 532-nm Perpendicular Channel. *Journal of Atmospheric and Oceanic Technology*. Vol. 26, 2015-2033. https://doi.org/10.1175/2009JTECHA1242.1.

[32] Yu, H., Chin, M., Winker, D. M., Omar, A. H., Liu, Z., Kittaka, C. and Diehl, T., (2010). Global View of Aerosol Vertical Distributions from CALIPSO Lidar Measurements and GOCART Simulations: Regional and Seasonal Variations. *Journal of Geophysical Research*. Vol. 115. https://doi.org/10.1029/2009JD013364.

[33] Gao, X. X., Chen, Y. and Zhang, W., (2016). Vertical Distribution Characteristics of Aerosols in North China From 2006 to 2015. *China Environmental Science*, Vol. 36, 2241-2250.

[34] Du, Z. and Wang, Y., (2022). Does Energy-Saving and Emission Reduction Policy Affects Carbon Reduction Performance? A Quasi-Experimental Evidence in China. *Applied Energy*. Vol. 3. https://doi.org/10.1016/j.apenergy.2022.119758.

[35] Oo, M. and Holz, R. E., (2011). Improving the CALIOP Aerosol Optical Depth Using Combined MODIS-CALIOP Observations and CALIOP Integrated Attenuated Total Color Ratio. *Journal of Geophysical Research*, Vol. 116. https://doi.org/10.1029/2010JD014894.

[36] Liu, Z., Fairlie, T. D., Uno, I., Huang, J., Huang, J., Wu, D., Omar, A., Kar, J., Vaughan, M. A., Rogers, R. R. R., Winker, D. M., Trepte, C. R., Hu, Y., Sun, W., Lin, B. and Cheng, A., (2013). Transpacific Transport and Evolution of the Optical Properties of Asian Dust. *Journal of Quantitative Spectroscopy and Radiative Transfer*, Vol. 116, 24-33. https://doi.org/10.1016/j.jqsrt.2012.11.011.

[37] Feng, X., Wei, S. and Wang, S., (2020). Temperature Inversions in the Atmospheric Boundary Layer and Lower Troposphere Over the Sichuan Basin, China: Climatology and Impacts on Air Pollution. *Science of The Total Environment*, Vol. 726. https://doi.org/10.1016/j.scitotenv.2020.138579.

[38] Lu, W., Liu, X., Liu, H. and Liu, C., (2024). Distinct Diurnal Characteristics of Summer Precipitation and Underlying Mechanisms in the Tibetan Plateau and Surrounding Basins. *Climate Dynamics*, Vol. 62,9405-9425. https://doi.org/10.1007/s00382-024-07338-4.

[39] Li, J., Chen, H., Jiang, X. and Li, P., (2024). Diurnal Variations of Summer Rainfall Response to Large-Scale Circulations and Low-Level Winds Over the Sichuan Basin. *Climate Dynamics*, Vol. 62,2041-2056. https://doi.org/10.1007/s00382-023-07009-w.